Analytic Non-Adiabatic Couplings for the Spin-Flip ORMAS Method

SCHOLARONE™
Manuscripts

Analytic Non-Adiabatic Couplings for the Spin-Flip ORMAS Method.

Joani Mato and Mark S. Gordon

Department of Chemistry and Ames Laboratory

Iowa State University, Ames, IA 50011

1. Abstract.

Analytic non-adiabatic coupling matrix elements (NACME) are derived and implemented for the spin-flip occupation restricted multiple active space configuration interaction (SF-ORMAS-CI) method. SF-ORMAS is a general spin correct implementation of the SF-CI method and has been shown to correctly describe various stationary geometries, including regions of conical intersections. The availability of non-adiabatic coupling allows a fuller examination of non-adiabatic phenomena with the SF-ORMAS method. In this study, the implementation of the NACME is tested using two model systems, MgFH and ethylene. In both cases, the SF-ORMAS method exhibits good qualitative agreement with established multi-reference methods, suggesting that SF-ORMAS is a suitable method for the study of non-adiabatic chemical phenomena.

2. Introduction.

The Born-Oppenheimer (BO) approximation allows each electronic state to be treated independently, while the nuclei move within the strict confines of a single BO potential energy surface (PES)[1]. This assumption greatly facilitates the quantum chemical study of molecules in their ground electronic states, for most of which the BO model is a sufficiently valid approximation. On the other hand, when two or more PESs approach degeneracy, the BO approximation no longer applies[2]. In such instances, the interaction between the various PESs becomes non-negligible, and energy can transfer readily between electronic and nuclear motions[2]. Transitions between BO states can occur via nuclear motion alone, thus allowing non-adiabatic processes to take place.

To account for the non-BO interaction between adiabatic states, it is often necessary to compute the first order vibronic couplings, otherwise known as *non-adiabatic coupling matrix elements* (NAC or NACME). The expression for the NACME between two states is given in equation (1):

$$D_{IJ}^x = \left\langle \Psi_I(r;X) \left| \frac{\partial}{\partial x} \right| \Psi_J(r;X) \right\rangle \tag{1}$$

In equation (1), Ψ_I and Ψ_J denote the adiabatic wave functions of states I and J, respectively, r denotes electronic coordinates, and X denotes the collection of nuclear coordinates, upon which the wave function depends parametrically. Lastly, the lowercase x in the derivative operator denotes an arbitrary nuclear coordinate. As implied in Eq. (1), the first order NACME is a vector quantity that depends on 3N cartesian coordinates, or 3N-6 internal coordinates (3N-5 for linear molecules), where N is the number of atoms. Hence, the first order NACME is sometimes referred to as a *vector* coupling[2].

The first order NACME is pivotal in the study of non-adiabatic phenomena, as the magnitude of the coupling often indicates the strength of the interaction between the two (or

more) adiabatic states[2,3], and by extension, the inappropriateness of the BO approximation. For example, in geometries for which two or more PESs are degenerate (regions of conical intersections), the NACME magnitude grows very large[4,5]. Moreover, the computation of the NACME has practical importance since it is often a required variable in minimum energy conical intersections (MECI) searches[6], and simulations of non-adiabatic dynamics[7,8].

While the availability of NACME is necessary in such cases, it is of equal importance that the underlying wave function used in Eq. (1) can accurately describe adiabatic PESs in the important regions of coordinate space. Traditionally, multi-reference (MR) methods have been used in non-adiabatic studies since they are best equipped to treat degeneracies or near-degeneracies. Commonly used methods are the multi-configurational self-consistent field (MCSCF)[9] and multi-reference configuration interaction (MRCI)[10] methods, both of which have analytic NACME available[3,11,12]. Multi-reference methods are ideal in the study of non-adiabatic processes; however, their computational expense limits these methods to relatively small systems. The MCSCF method may also exhibit convergence and root-flipping issues[13], in addition to the need to carefully select an active space for the system of interest.

An attractive alternative to MR treatments are the spin-flip (SF) family of methods, introduced by Krylov[14–16]. Adapted to a variety of quantum chemical schemes such as configuration interaction (SF-CI)[15,17], equations-of-motion coupled-cluster (SF-EOM)[14], and time-dependent density functional theory (SF-TDDFT)[18], SF methods have been used to adequately describe non-dynamic correlation, particularly in regions of conical intersections[19–21]. Analytic gradients[22] and analytic NACME[23] have also been derived and implemented for some of the SF methods. However, many SF methods suffer from unpredictable spin-contamination since the wave function is not an exact eigenfunction of the $\hat{S}^2$ operator[24]. This somewhat limits the usefulness of the above-mentioned SF schemes. As a

result, several schemes restoring spin-completeness of the SF configurational space have been implemented within wave function theory[17,25–27] and TDDFT[28–31].

The SF-ORMAS[32] family of methods was developed as a *general* SF configuration interaction approach that corrects the spin-contamination present in conventional SF-CI methods. SF-ORMAS was shown to correctly capture non-dynamic correlation in such processes as bond-breaking, diradical transition states, and low-lying excited states. An analytic gradient was also developed[33], allowing for the efficient optimization of minima, transition states, and conical intersections. The molecular structures optimized at the SF-ORMAS level of theory were in most cases very similar to the structures optimized by multi-reference methods such as MRCI and MRPT2.

In the present paper the analytic NACME for SF-ORMAS is derived and implemented in the GAMESS (General Atomic and Molecular Electronic Structure System)[34,35] quantum chemistry software package.

3. Theoretical Approach

2.1 A brief overview of the SF-ORMAS method

A brief overview of the SF-ORMAS method is given here for completeness. Readers who are interested in a more detailed description of the method are directed to the original SF-ORMAS paper[32].

SF-ORMAS is a general single-reference spin-flip configuration interaction (SF-CI) method[15,17,24]. Unlike conventional CI methods, SF-CI is performed through a series of spin-flipping excitations from a high-spin open-shell determinant (ROHF in this case), resulting in determinants with a lower $\hat{S}_Z$ eigenvalue than the original SCF calculation (i.e. $\Delta M_s < 0$). This results in a CI wave function that has a lower multiplicity than the underlying SCF calculation. For example, a single SF-CIS calculation requires a triplet starting determinant to produce a

final singlet CI wave function. A graphical representation of the SF-CIS procedure is shown in
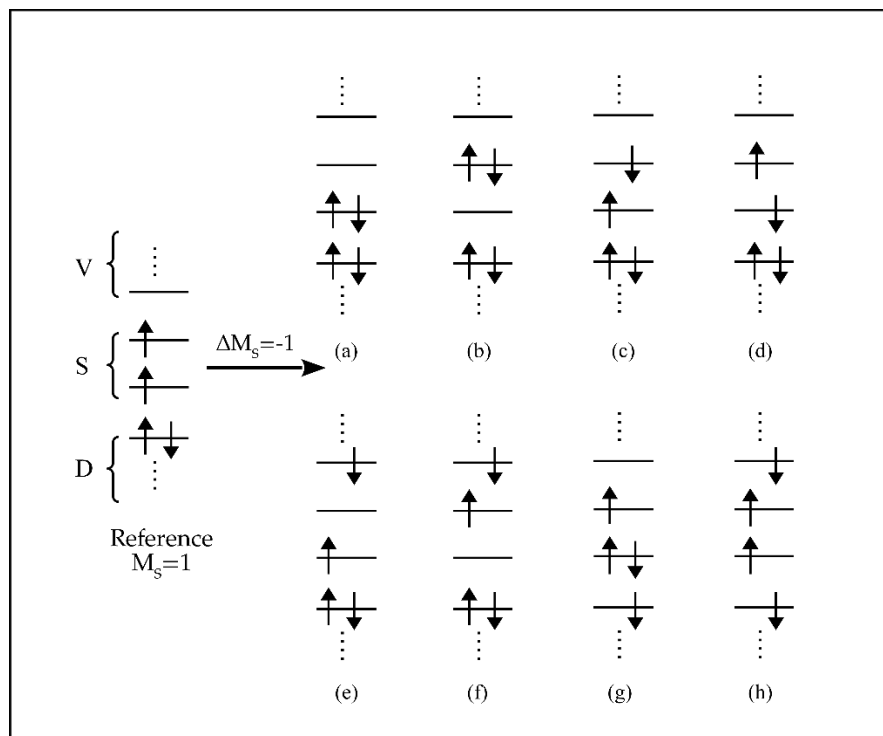
Figure 1.

Figure 1: A graphical representation of the SF-CIS procedure

Because of the high-spin starting determinant, spin-flip methods provide a multi-

reference description of the system within a single-reference formalism (only a single

determinant is used as the starting point). This offers significant advantages in computational

efficiency and accuracy but suffers from the unfortunate side-effect of spin-contamination.

The wave function generated by the spin-flip procedure is an eigenfunction of the $\hat{S}_Z$ operator,

but not necessarily of the $\hat{S}^2$ operator. This is evident in Figure 1, as determinants (e), (f), (g),

and (h) cannot be paired into configuration state functions (CSFs).

The SF-ORMAS method was developed as a solution to the spin-contamination

problem of SF-CI, as well as an attempt to generalize all currently available SF-CI schemes into

one unified method. The SF-ORMAS method relies on the powerful ORMAS algorithm[36], which

allows for the arbitrary partitioning of the orbital space into subspaces, each constrained by a

minimum and maximum number of electron occupations. The SF-ORMAS procedure imposes the additional constraint that each generated determinant must be of a lower multiplicity than the underling SCF determinant. While the ORMAS method also relies on Slater determinants rather than CSFs, it generates all possible determinants within the given set of constraints. As such, the final SF-ORMAS wave function possesses the correct spin symmetry and does not suffer from spin-contamination.

Many possible SF-CI schemes are available through the SF-ORMAS procedure, many of which are exemplified in the previous publications of the method[32,33]. The SF-ORMAS method also includes analytic gradients[33] for geometry optimizations, as well as a perturbation correction to account for dynamic correlation[32].

2.2 Analytic expressions for the SF-ORMAS NACME

SF-ORMAS is a general CI method; therefore, the derivation of the analytic NACME is formally identical to that of MCSCF/MRCI[3,37], with the main differences occurring in the response terms. Thus, only a brief summary of the derivation is presented below. To maintain the generality of the SF-ORMAS method, no assumptions are made about the occupation or partitions of the ORMAS subspaces in this derivation, other than the required "spin-flipping" constraint. Thus, in principle, this derivation is applicable to every SF-ORMAS partitioning scheme that has been previously introduced[32,33].

The total SF-ORMAS wave function for an arbitrary CI state I can be expressed as a linear combination of Slater determinants:

$$\Psi_I = \sum_t C_t^I \psi_t \tag{2}$$

In equation (2), ψ_t denotes the Slater determinants, C_t^I the variationally optimized CI coefficients for state I, while the index t runs over all possible determinants in a given CI

expansion. Nuclear and electronic coordinate dependencies have been left out of the above

notation for simplicity. Applying Eq. (2) to the NACME definition (1) results in the two-term

equation:

$$D_{IJ}^x = \left\langle \sum_t C_t^I \psi_t \middle| \sum_{t'} \frac{\partial C_{t'}^J}{\partial x} \psi_{t'} \right\rangle + \left\langle \sum_t C_t^I \psi_t \middle| \sum_{t'} C_{t'}^J \frac{\partial \psi_{t'}}{\partial x} \right\rangle = D_{IJ}^{x,CI} + D_{IJ}^{x,MO} \qquad (3)$$

Thus, the computation of the analytic NACME is split into two terms, one containing the

derivatives of the CI coefficients (the CI term), and one containing the derivatives of the Slater

determinant (hereafter referred to as the MO term).

The CI term can be simplified by taking advantage of the orthonormality between

Slater determinants:

$$D_{IJ}^{x,CI} = \sum_{tt'} C_t^I \frac{\partial C_{t'}^J}{\partial x} \langle \psi_t | \psi_{t'} \rangle = \sum_t C_t^I \frac{\partial C_t^J}{\partial x} = \mathbf{C}^I {}^\dagger \frac{\partial}{\partial x} \mathbf{C}^J \qquad (4)$$

where a bold typeface in Eq. (4) represents a vector quantity. The direct differentiation of the

CI coefficients in Eq. (4) can be avoided by manipulating the coupled-perturbed CI

equations[38]. By differentiating the CI variational condition, $\mathbf{HC} - \mathbf{EC} = \mathbf{0}$, the expression in Eq.

(4) can be written as:

$$\mathbf{C}^I {}^\dagger \frac{\partial}{\partial x} \mathbf{C}^J = (E_I - E_J)^{-1} \mathbf{C}^I {}^\dagger \frac{\partial \mathbf{H}}{\partial x} \mathbf{C}^J \qquad (5)$$

where E_I and E_J are the energies of states I and J, and $\mathbf{H}$ represents the *Hamiltonian matrix*

elements between Slater determinants. The derivative term on the right hand side of Eq. (5)

reduces to an expression very similar to that of the CI gradient[33,39]:

$$\mathbf{C}^I {}^\dagger \frac{\partial \mathbf{H}}{\partial x} \mathbf{C}^J = \sum_{ij}^{MO} Q_{ij}^{IJ} h_{ij}^x + \sum_{ijkl}^{MO} G_{ijkl}^{IJ} (ij|kl)^x + \sum_{ij}^{MO} L_{ij}^{IJ} U_{ij}^x \qquad (6)$$

The sums on the right-hand side of equation (6) run over all molecular orbitals (MOs).

Eq. (6) and the analytic gradient expression for the CI energy differ in the densities and

lagrangian expressions. The one- and two-particle densities, and the CI lagrangian in the CI

gradient expression are replaced by the corresponding transition densities (Q_{ij}^{IJ} and G_{ijkl}^{IJ}) and

the transition lagrangian (L_{ij}^{IJ}), respectively.

The transition densities are defined by:

$$Q_{ij}^{IJ} = \sum_{tt'} C_t^I Q_{ij}^{tt'} C_{t'}^J \;\; ; \;\; G_{ijkl}^{IJ} = \sum_{tt'} C_t^I G_{ijkl}^{tt'} C_{t'}^J \tag{7}$$

where $Q_{ij}^{tt'}$ and $G_{ijkl}^{tt'}$ in Eq. (7) are the CI coupling constants for two arbitrary Slater

determinants t and t'.

The transition lagrangian is defined by:

$$L_{ij}^{IJ} = 2\sum_p^{MO} Q_{ip}^{IJ} h_{jp} + 4\sum_{pqs}^{MO} G_{ipqs}^{IJ}(jp \mid qs) \tag{8}$$

where h_{jp} and $(jp \mid qs)$ are the one and two-electron integrals in the MO basis, respectively.

The remaining terms in Eq. (6) are identical to those used in the CI analytic gradients,

provided that states I and J use a common set of molecular orbitals (which is the case in SF-

ORMAS). The terms h_{ij}^x and $(ij \mid kl)^x$ are the "skeleton" one- and two-electron integrals,

defined by:

$$h_{ij}^x = \sum_{\mu\nu}^{AO} c_{i\mu}c_{j\nu}\frac{\partial h_{\mu\nu}}{\partial x}$$

$$\tag{9}$$

$$(ij \mid kl)^x = \sum_{\mu\nu\rho\sigma}^{AO} c_{i\mu}c_{j\nu}c_{k\rho}c_{l\sigma}\frac{\partial(\mu\nu|\rho\sigma)}{\partial x}$$

where $h_{\mu\nu}$ and $(\mu\nu|\rho\sigma)$ are the one- and two-electron integrals in the atomic orbital (AO)

basis, and $c_{i\mu}$ are the MO coefficients. Lastly, U_{ij}^x in Eq. (6) are the MO response terms,

determined via the coupled-perturbed Hartree-Fock (CPHF) equation.

The derivative with respect to Slater determinants in the NACME expression (3), i.e. the MO term, reduces to the derivative of molecular orbitals by recognizing that a derivative works as a one-electron operator. This expression then takes the form:

$$D_{IJ}^{x,MO} = \sum_{ij}^{MO} Q_{ij}^{IJ} \left\langle \phi_i \left| \frac{\partial}{\partial x} \right| \phi_j \right\rangle \tag{10}$$

where ϕ_i denotes the molecular orbitals and Q_{ij}^{IJ} is an element of the transition one-particle density matrix, defined in Eq. (7). Since the molecular orbitals are expanded in atomic orbitals via the expression, $\phi_i = \sum_\mu c_{i\mu} \chi_\mu$, the derivative in Eq. (10) is expanded by the product rule into the derivatives of atomic orbitals and MO coefficients (expressed through the response terms, as above). Thus, the final form of the MO term becomes:

$$D_{IJ}^{x,MO} = \sum_{ij}^{MO} Q_{ij}^{IJ} \left[\sum_{\mu\nu}^{AO} c_{i\mu} c_{j\nu} \left\langle \chi_\mu \left| \frac{\partial}{\partial x} \right| \chi_\nu \right\rangle + \sum_p^{MO} S_{ip} U_{pj}^x \right] = \sum_{ij}^{MO} Q_{ij}^{IJ} \left[\sigma_{ij}^x + U_{ij}^x \right] \tag{11}$$

where $S_{ip} = \langle \phi_i | \phi_p \rangle$ in Eq. (11) is the overlap matrix of the orthonormal MOs.

The total expression for the NACME is written as:

$$\begin{aligned}
D_{ij}^x &= (E_I - E_j)^{-1} \left[\sum_{ij}^{MO} Q_{ij}^{IJ} h_{ij}^x + \sum_{ijkl}^{MO} G_{ijkl}^{IJ} (ij|kl)^x + \sum_{ij}^{MO} L_{ij}^{IJ} U_{ij}^x \right] + \sum_{ij}^{MO} Q_{ij}^{IJ} \left[\sigma_{ij}^x + U_{ij}^x \right] \\
&= (E_I - E_j)^{-1} \left[\sum_{ij}^{MO} Q_{ij}^{IJ} h_{ij}^x + \sum_{ijkl}^{MO} G_{ijkl}^{IJ} (ij|kl)^x \right] \\
&\quad + \sum_{ij}^{MO} \left[\{ L_{ij}^{IJ} (E_I - E_J)^{-1} + Q_{ij}^{IJ} \} U_{ij}^x + Q_{ij}^{IJ} \sigma_{ij}^x \right]
\end{aligned} \tag{12}$$

As in the case of the SF-ORMAS analytic gradients, the MO responses must reflect the underlying open-shell high-spin SCF calculations[33], as well as the specific partitioning of the orbital space by the ORMAS algorithm (the total energy is invariant to orbital rotations within the same ORMAS subspace). Specifically, the MO responses in Eq. (12) are obtained through

the solution of the coupled-perturbed ROHF (CPROHF) equations, which can be formally derived by differentiating the ROHF variational condition[38,40]. The CPROHF equations are concisely written as:

$$AU^x = B^x \tag{13}$$

The matrix A is the orbital hessian, and B^x depends on the derivatives of the Fock and overlap matrices. The exact expressions for these matrices have been reported abundantly throughout the literature[38,40–42], so they are not reproduced here. Eq. (13) requires that each response is solved for all 3N (or 3N-6) degrees of freedom in a molecular system. This can be avoided by applying the Z-vector method of Handy and Schaefer[43]. First, it is recognized that the response terms U_{ij}^x are subject to the orthonormality condition:

$$U_{ij}^x + U_{ji}^x + S_{ij}^x = 0 \tag{14}$$

The last term in Eq. (14) is the derivative of the overlap matrix. The sum containing the response term in the NACME expression of Eq. (12) may be manipulated further by using the orthonormality condition of Eq. (14) to obtain:

$$\sum_{ij}^{MO} \left\{ L_{ij}^{IJ}(E_I - E_J)^{-1} + Q_{ij}^{IJ} \right\} U_{ij}^x = \sum_{ij}^{MO} T_{ij}^{IJ} U_{ij}^x$$

$$= \frac{1}{2}\sum_{ij}^{MO} T_{ij}^{IJ}(U_{ij}^x + U_{ji}^x) + \frac{1}{2}\sum_{ij}^{MO} T_{ij}^{IJ}(U_{ij}^x - U_{ji}^x) = \frac{1}{2}\sum_{ij}^{MO}(T_{ij}^{IJ} - T_{ji}^{IJ})U_{ij}^x - \frac{1}{2}\sum_{ij}^{MO} T_{ij}^{IJ}S_{ij}^x \tag{15}$$

The term $T_{ij}^{IJ} = L_{ij}^{IJ}(E_I - E_J)^{-1} + Q_{ij}^{IJ}$ has been defined. Eq. (15) requires only the unique elements of the response term (i.e. the orbital pairs for which the energy is not invariant). In a SF-ORMAS calculation, this involves pairs of orbitals between different ORMAS subspaces[36]. By inverting Eq. (13) and applying the resulting expression to Eq. (15), one obtains the Z-vector equation:

$$A^T Z^{IJ} = \Delta T^{IJ} \tag{16}$$

ΔT^{IJ} is defined as $\Delta T^{IJ} = T^{IJ}_{ij} - T^{IJ}_{ji}$. Finally, the Z-vector solution of Eq. (16) can be used in the NACME expression in Eq. (12) to obtain:

$$\frac{1}{2}\sum_{ij}^{MO}\Delta T^{IJ}U^x_{ij} = \frac{1}{2}\sum_{ij}^{indep.} Z_{ij}B^x_{ij} \tag{17}$$

The sum on the right-hand side of Eq. (17) runs only over independent orbital pairs, for which the energy is not invariant to rotations.

4. Implementation and testing

Most terms for the SF-ORMAS NACME expression are readily available from the recently implemented analytic gradients[33] in GAMESS. The only novel terms are the transition density matrices which may be formed using the existing ORMAS routines. The transition densities are obtained through the use of the Slater-Condon rules[44–46] by looping over all possible single and double excitations to generate the coupling constants, and then multiplying by the CI coefficients from the two states[36,47].

To test the implementation of the analytic NACME for SF-ORMAS, numeric non-adiabatic couplings via finite differencing were also coded in GAMESS. Starting from Eq. (3), the CI and MO terms of the NACME can be written as numerical derivatives in the following way, respectively[48]:

$$\sum_t C^I_t\frac{\partial}{\partial x}C^J_t = \sum_t \frac{C^I_t \cdot C^{J,\,+\Delta x}_t - C^I_t \cdot C^{J,\,-\Delta x}_t}{2\Delta x} \tag{18}$$

$$\sum_{ij}^{MO}Q^{IJ}_{ij}\left\langle\phi_i\left|\frac{\partial}{\partial x}\right|\phi_j\right\rangle = \sum_{ij}^{MO}Q^{IJ}_{ij}\frac{\left\langle\phi_i\,\middle|\,\phi_j^{+\Delta x}\right\rangle - \left\langle\phi_i\,\middle|\,\phi_j^{-\Delta x}\right\rangle}{2\Delta x} \tag{19}$$

In Eqs. (18) and (19), the double difference formula is used to approximate the nuclear derivatives. The superscripts '$+\Delta x$' and '$-\Delta x$' denote quantities computed at a displaced cartesian geometry, either positive or negative by an amount Δx.

Eq. (18) requires that the original (not displaced) set of CI coefficients always be available at each displaced geometry in order to compute the CI overlaps. However, no more than two sets of CI coefficients need to be stored in disk or memory at any given displacement. Similarly, the displaced MO overlap in Eq. (19) requires the displaced AO overlap matrix ($\langle \chi_\mu | \chi_v^{\Delta x} \rangle$), as well as the MO coefficients, computed at two different geometries.

A major concern in the evaluation of the numerical NACME is the phase of the wave function. The total energy and energy derivatives of the system are not susceptible to changes in the phase of the MO and/or CI coefficients; the numerical NACMEs in Eqs. (18) and (19), on the other hand, are not invariant to phase changes between displacements.

To avoid this problem, the phase consistency of the MO coefficients was ensured by monitoring the diagonal elements of the displaced MO overlaps, $S_{ii}^{\Delta x} = \langle \phi_i | \phi_i^{\Delta x} \rangle$. Provided that Δx is sufficiently small, the displaced overlap should be close to 1 if no change of phase has occurred, and close to -1, if a change of phase has occurred. Thus, multiplying each new molecular orbital, $\phi_i^{\Delta x}$ by the quantity, $\frac{S_{ii}^{\Delta x}}{|S_{ii}^{\Delta x}|} = \pm 1$ ensures that all MOs maintain the same phase between displacements. A similar procedure was carried out for the CI coefficients as well. To minimize the complexity of the CI phase, the MO phases were corrected (when necessary) immediately after the SCF step of the SF-ORMAS calculation, but *before* the CI step. Finally, the antisymmetric nature of the derivative operator (and consequently of the NACME) was used as a test of accuracy during the coding process of the numerical NACME. After several trials, a value of 0.005 bohr was chosen as an optimal value for the displacement variable, Δx, to avoid potential numerical instabilities.

The analytic NACME implementation was compared to the numerical NACME, and in most cases the agreement between the two is on the order of $10^{-5} - 10^{-6}$ bohr^{-1}. In some cases,

agreement only on the order of 10^{-4} could be achieved. Since the numerical differentiation

happens along cartesian coordinates, any displacements that change the molecular center of

mass have the potential to introduce minor errors into the evaluation of the numerical

NACME.

5. Illustrative calculations

To illustrate the implementation of the NACME for the SF-ORMAS method, examples with

MgFH and ethylene are considered in this study. These are compared with MCSCF calculations

of the state-averaged complete active space kind[49–51] (SA-CASSCF), for which NACME have

already been implemented in GAMESS. Since all CASSCF calculations employed in this study

are state-averaged, the SA prefix is implied and therefore not used in the rest of this paper.

Two different SF-ORMAS schemes are used throughout these examples: the SF-

ORMAS-CIS (i.e. allowing single excitations into the virtual space), and SF-CAS (no excitations

into the virtual space)[32]. Additionally, single spin-flip (1SF) and double spin-flip (2SF)

examples are considered. Unless otherwise stated, all calculations in this section use the 6-

31G(d) basis set.

MgFH

The first example considered for the SF-ORMAS NACME is the reaction

$Mg + HF \rightarrow MgF + H$. Following the example of Saxe, Lengsfield, and Yarkony[11], the couplings

of the reaction are calculated along the collinear surface of Mg – F – H in which the distance

between hydrogen and fluorine is varied. Along this path, the reaction exhibits charge

transfer between the σ and σ^* orbitals of the H-F bond. Only the two lowest $^1\Sigma^+$ states of the

system are considered here.

First, the SF-ORMAS calculations are compared with those of the CASSCF method to ensure that the quality of the two wave functions is comparable for the purposes of this investigation. Two SF schemes are considered for this system, the SF-ORMAS-CIS, and SF-CAS(2,2).

Similarly, two different active spaces are used in the CASSCF calculation: a minimal (2,2) space which contains only the σ and σ^* HF orbitals, and a larger (4,6) active space, containing the aforementioned σ orbitals, the magnesium 3s and 3p (x and y) orbitals, as well as the fluorine $3p_z$ orbitals. All atoms of the MgFH molecule are located along the z-axis.

Figure 2 shows a potential energy surface scan along the H-F bond distance for the $1\,^1\Sigma^+$ and $2\,^1\Sigma^+$ states of the Mg-F-H system at four different levels of theory. Figure 3 shows the energy difference (calculated as $2\,^1\Sigma^+ - 1\,^1\Sigma^+$) along the same bond distances.
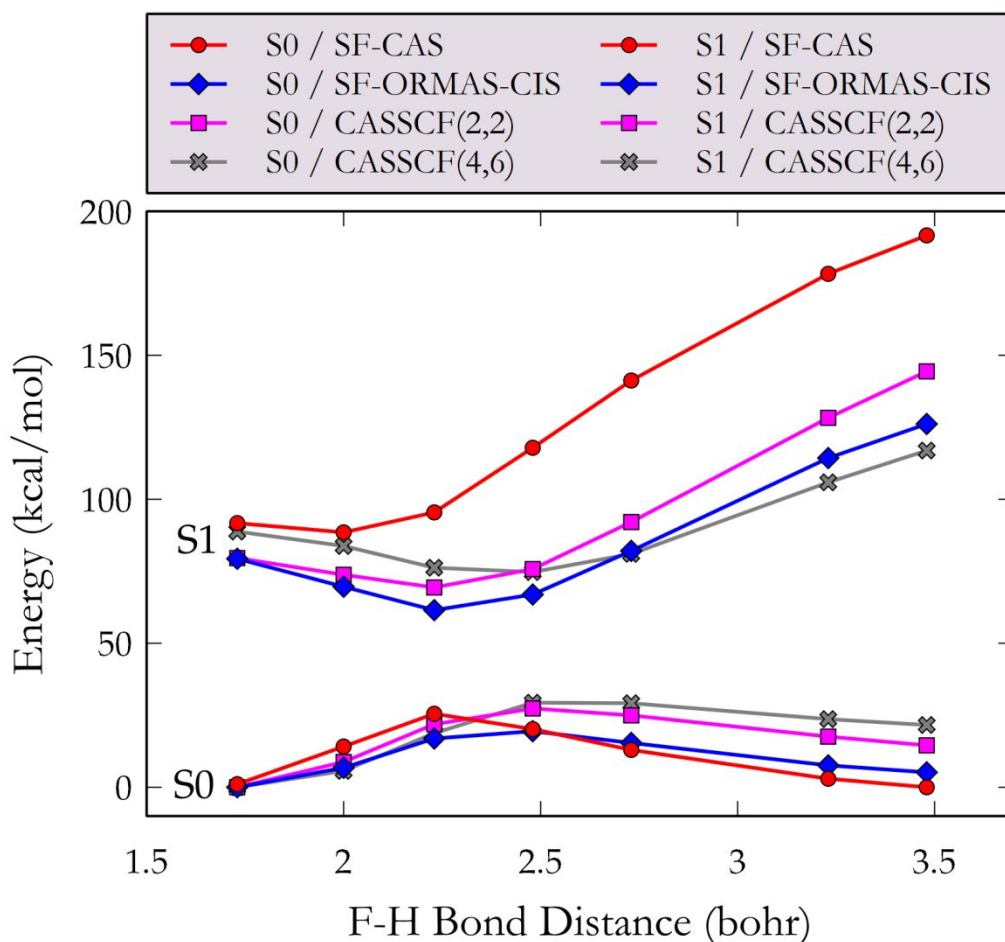
Figure 2: A PES scan along the F-H distance (in bohr) of the Mg-F-H complex for the two lowest $^1\Sigma^+$ states. All

methods use the 6-31G(d) basis set. All methods share a common 0 kcal/mol energy in the ground state PES.
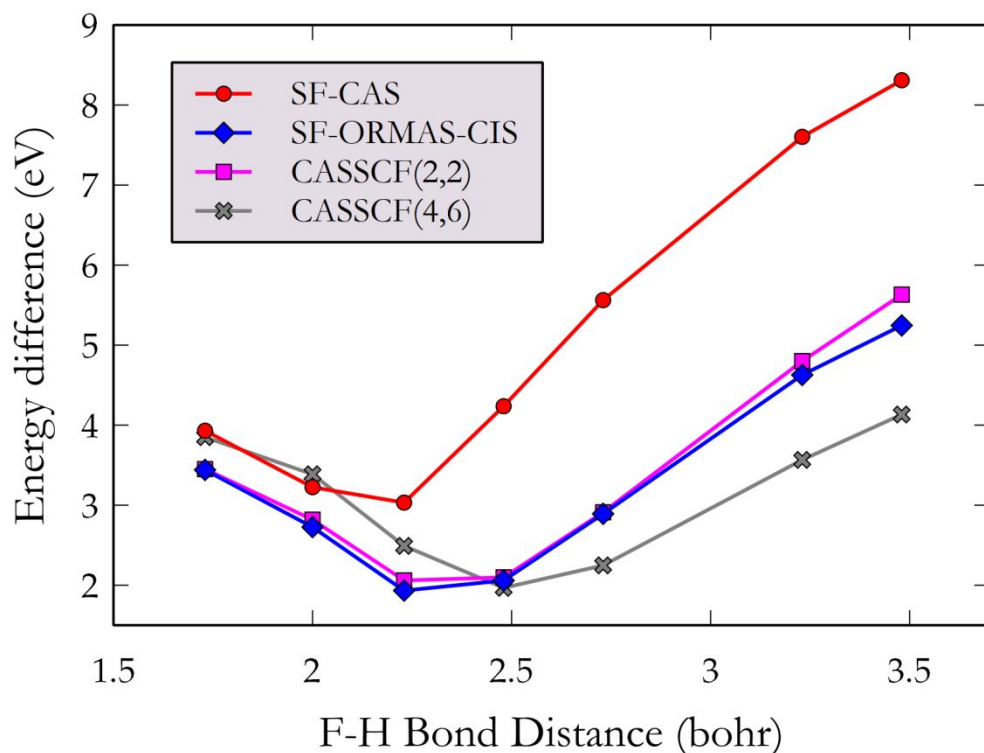
Figure 3: The energy difference (in eV) between the two lowest $^1\Sigma^+$ states of the Mg – F – H complex as a function of the F-H distance (in bohr).

The ground state potential energy surfaces show little difference among the four

levels of theory presented in Figure 2. All methods produce qualitatively similar PESs,

displaying significant overlap and successfully capturing the small barrier present along the

bond elongation path. On the other hand, the excited state potential energy curves obtained

using the four different methods are appreciably different, particularly the curve generated by

the SF-CAS method. While qualitatively similar to the other methods, SF-CAS greatly

overestimates the energy of the $2\ ^1\Sigma^+$ state at large H-F distances, as demonstrated in Figure

3. While the difference is mostly quantitative (the general trend of the PES remains similar to

that of the other methods), the lower quality of the SF-CAS wave function in this instance is

understandable since the method lacks additional excitations into the virtual space which are

crucial for the characterization of the $2\,^1\Sigma^+$ excited state. The CASSCF(2,2) method also lacks

such excitations; however, the orbital optimization (not present in SF methods) along with

the state-averaging work to reduce the impact of the lack of excitations into the virtual space.

Similarly, the additional single excitations present in the SF-ORMAS-CIS method (not included

in SF-CAS) significantly improve the description of the excited state. As Figure 3 shows, the

SF-ORMAS-CIS excitation energies along the PES are virtually identical to those of

CASSCF(2,2).

The inclusion of the σ and σ^* orbitals in the active space is critical for the description

of the charge-transfer nature of the reaction. Indeed, all methods contain the σ orbitals in

their active space (in SF methods, the "active space" is the singly occupied space of the ROHF

reference[32]). Figure 4 shows the natural orbital occupation numbers (NOON, computed by

diagonalizing the state specific density matrix) of the σ and σ^* orbitals along the F – H bond

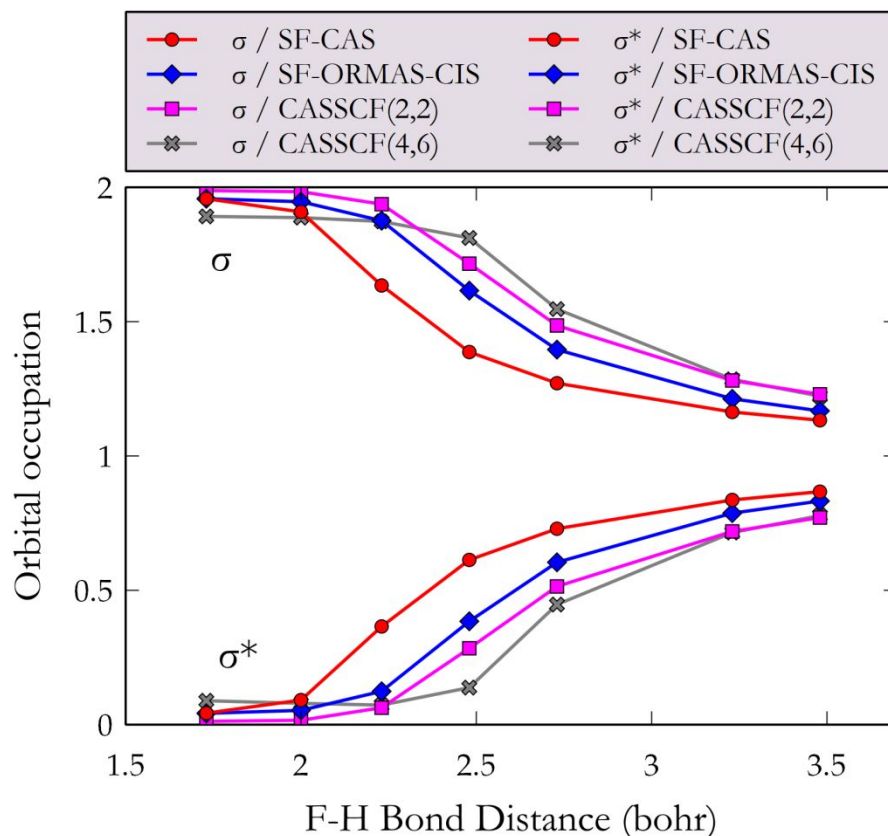elongation, calculated at the same levels of theory.

Figure 4: The natural orbital occupation numbers of the σ and σ* orbitals along the F – H bond elongation coordinate. All methods use the 6-31G(d) basis set.

Figure 4 demonstrates the excellent qualitative agreement between the SF-ORMAS and the CASSCF NOON. At smaller bond distances the occupation of the σ orbital is near 2.0, while the occupation of the σ^{*} orbital is near 0.0. As the bond elongates, electron density transfers from the σ to the σ^{*} orbital, until the occupations of the two orbitals approach 1.0. Once again, the SF-CAS method deviates slightly from the other methods as the occupation change happens at smaller distances. This is again attributed to the inflexibility of the SF-CAS wave function, as the open shell triplet reference used in SF methods strongly favors the diradical configuration. Both SF-ORMAS methods employed here agree qualitatively with the CASSCF results.

Table 1 shows the absolute values of the NACME for several F-H distances, computed

at all four levels of theory discussed above. The NACME in cartesian coordinates is a vector of

dimension 3N (where N is the number of nuclei). However, in this case the NACME along the x

and y coordinates vanish because of linearity and the fact that both states belong to the totally

symmetric irreducible representation of the $D_{\infty h}$ group ($^1\Sigma^+$). Therefore, only the non-

vanishing NACME along the z-direction (molecular axis) are given in Table 1. For small

systems like MgFH it is possible to make a direct comparison of the NACME along the

symmetry unique coordinates.

Table 1: The absolute value of the NACME z-component (in bohr^{-1}) as a function of the F-H distance (in bohr).

F-H distance	CASSCF(2,2)			CASSCF(4,6)			SF-ORMAS-CIS			SF-CAS-CI		
	Mg	F	H	Mg	F	H	Mg	F	H	Mg	F	H
1.73	0.364	0.264	0.217	0.330	0.177	0.158	0.371	0.245	0.196	0.442	0.300	0.213
2.00	0.373	0.769	0.661	0.305	0.515	0.490	0.369	0.836	0.703	0.560	1.586	1.314
2.23	0.513	1.734	1.426	0.367	1.122	0.974	0.538	1.939	1.582	0.409	1.543	1.323
2.48	0.480	1.604	1.290	0.515	1.708	1.365	0.485	1.636	1.309	0.199	0.552	0.494
2.73	0.268	0.725	0.599	0.449	1.201	0.910	0.274	0.733	0.601	0.119	0.232	0.228
3.23	0.110	0.178	0.179	0.224	0.353	0.258	0.115	0.218	0.203	0.060	0.066	0.086
3.48	0.082	0.100	0.118	0.181	0.223	0.158	0.113	0.159	0.094	0.046	0.040	0.062

All methods show the same general trend along the elongation of the H-F bond. The

NACME values in Table 1 appear to be *inversely related to the energy difference* between the

two $^1\Sigma^+$ states. For example, at an F-H distance of 2.23 bohr, both the SF-ORMAS-CIS method

and the CASSCF(2,2) method exhibit the smallest energy gap between the two states (see

Figure 3), and consequently the largest magnitude of the NACME for each atom (Table 1). At

the point of largest energy separation (a distance of 3.48 bohr), the NACME values are

consistently the smallest for all methods. The magnitude of the NACME is expected to be

inversely related to the energy difference between two states[2]. This relationship is formally

exact for exact wave functions, although only approximate for approximate wave functions, as

shown in Eqs. (5) and (12). Nevertheless, this trend holds very well for CI wave functions, as

the CI contribution to the NACME is often the largest[48,52].

Table 2 shows the norm of the NACME (|NACME|, defined as the usual norm for a 3N-

dimensional vector; i.e. $|D| = \sqrt{\sum_i^{3N} D_i^2}$) multiplied by the energy difference between the two

states.

Table 2: Norm of the NACME multiplied by the energy difference between the two $^1\Sigma^+$ states (i.e. $|NACME| * \Delta E$)
in units of eV/bohr. The HF bond distance is in units of bohr.

HF Distance	$\|NACME\| * \Delta E$			
	CASSCF(2,2)	CASSCF(4,6)	SF-ORMAS-CIS	SF-CAS-CI
1.73	1.724608519	1.566863645	1.670905953	2.261304065
2.00	3.045000722	2.620178643	3.1428818	6.883013323
2.23	4.743683976	3.813668526	4.948593597	6.286231137
2.48	4.435114396	4.418846852	4.427928061	3.24986534
2.73	2.8482491	3.5354586	2.854074715	1.923755155
3.23	1.322232239	1.753217834	1.47917789	0.943628098
3.48	0.987176005	1.355925724	1.136395302	0.724298597

The values in Table 2 take into account both the NACME as well as the energy

difference between the two states considered. The $|NACME| * \Delta E$ values for SF-ORMAS-CIS

follow consistently the same pattern as the values for CASSCF(2,2) and CASSCF(4,6), in most

cases landing somewhere between the two (Table 2). The accuracy of single spin-flip CI is

expected to be approximately at the level of CASSCF(2,2), and the values in Table 2 do indeed

reflect that assertion. SF-CAS, on the other hand, appears to overestimate the $|NACME| * \Delta E$

value at short H-F distances, and underestimate it at long H-F distances. Nevertheless, SF-CAS

also follows roughly the same pattern as the other three methods shown in Table 2.

The similar qualitative behavior of the SF-ORMAS non-adiabatic couplings with those

of CASSCF suggest the suitability of the SF-ORMAS method in the study of such systems. The

differences in the NACME values between SF-ORMAS and CASSCF reflect their differences in

the description of the PES.

Ethylene

The ethylene molecule (C_2H_4) is a classic example of a system that can illustrate the influence

of conical intersections in organic chemistry. The first $\pi\pi^*$ excited state of ethylene has a

short lifetime and undergoes rapid isomerization[53]. Generally, the analysis of ethylene at non-

equilibrium geometries at which the adiabatic approximation is not appropriate requires a

multi-reference approach; however, spin-flip methods have proven to be adequate in the

treatment of ethylene near a conical intersection[42]. SF-ORMAS in particular was shown to

predict energies and geometries comparable to those obtained using multi-reference

methods, such as MRCI and MRPT2, at multiple stationary points on the ethylene PES,

including minima, saddle points, and minimum energy conical intersections (MECI)[32,33].

Table 3 shows the norm of the NACME (|NACME|, defined as the usual norm for a 3N-

dimensional vector; i.e. $|D| = \sqrt{\Sigma_i^{3N} D_i^2}$) for several levels of theory computed at three critical

geometries of ethylene: the D_{2h} ground state geometry, the D_{2d} rotational transition state, and

the twisted-pyramidal S1/S0 conical intersection geometry[53]. The norm of the NACME vector

(instead of individual cartesian coordinates) is used to simplify the comparison among the

different levels of theory. The norm of the NACME is used in the calculation of transition

probabilities between states in the adiabatic representation[55].

Table 3 also shows the difference in energy between the ground state (S0) and first

excited state (S1) in each respective geometry.

Table 3: |NACME| (in bohr^{-1}) and energy difference (in eV) between the ground and first excited state of ethylene calculated at three different geometries. All methods use the 6-31G(d) basis set. The MRCI calculations use CASSCF(2,2) as a reference. The energy difference at the MECI was confirmed to be negligible (~0 eV) and is therefore not given. The quantities of |NACME| $* \Delta E$ (in units of eV/bohr) are also given for the ground state and transition state geometries.

Geom. Method	Ground state (D$_{2h}$)			Trans. state (D$_{2d}$)			MECI
	ΔE(S1-S0)	|NACME|	|NACME|* ΔE	ΔE(S1-S0)	|NACME|	|NACME|* ΔE	|NACME|
CASSCF(2,2)	10.2	0.416	4.24	4.2	0.703	2.95	3.8×10^4
CASSCF(4,4)	9.6	0.351	3.37	3.9	0.702	2.74	5.6×10^4
SF-CAS(2,2)	11	0.374	4.11	6.5	0.463	3.01	2.4×10^4
2SF-CAS(4,4)	10.3	0.300	3.09	5.6	0.484	2.71	4.7×10^3
SF-ORMAS-CIS	9.0	0.330	2.97	3.4	0.870	2.96	3.7×10^5
MRCISD	9.2	0.345	3.174	3.5	0.674	2.36	N/A

The NACME norms computed here are in good qualitative agreement among the

different levels of theory. As shown in Table 3, the transition state geometry (located at a 90°

HCCH torsional angle) displays NACME norms with magnitudes that are consistently larger

than those of the ground state geometry. The NACME norms calculated via SF-CAS (with

either single or double spin-flip) are consistently smaller than their CASSCF counterparts.

This is expected given the disparity in the excitation energies calculated by the two families of methods (see Table 3). Since SF-CAS produces higher excitation energies, it is reasonable that the computed NACME norms will be lower in magnitude. Indeed, the norm of the NACME multiplied by the energy difference (shown for the ground state and transition state geometries in Table 3) for all methods are within ~1 eV/bohr of each other.

Considering that neither SF-CAS nor CASSCF account for dynamic correlation, state-averaged CASSCF tends to underestimate excitation energies, whereas SF-CAS tends to overestimate them. It has been shown that adding dynamic correlation via perturbation theory (i.e. SF-MRMP2)[32] significantly improves the excitation energies for SF-CAS. However, the NACME norms calculated at the SF-CAS level of theory are likely to be smaller than the corresponding CASSCF values at geometries that have non-negligible excitation energies, due to the tendency of SF-CAS to overestimate such energies. The difference is quantitative, however, as both methods obey the same general trend. For instance, at their respective MECI geometries at which the two states are degenerate, both methods show very large NACME norms with little significant differences among the various methods.

Inclusion of additional single excitations, as in the SF-ORMAS-CIS method, significantly improves not only the excitation energies, but also the NACME norms. At the ground state geometry, the NACME norms for SF-ORMAS-CIS are very close to both CASSCF methods and MRCI (while the excitation energy is much closer to that of MRCI). The same is true for the transition state geometry. In the transition state geometry (D_{2d} symmetry) there is a slightly greater disparity in the NACME norms between SF-ORMAS-CI and MRCI, attributed to the additional double excitations present in the MRCI method.

As expected, the SF-ORMAS method behaves qualitatively similarly to both CASSCF and MRCI in the computation of non-adiabatic couplings. In conjunction with previous energy

and geometry calculations[32,33], SF-ORMAS methods show great promise in the study of non-adiabatic processes for organic molecules.

6. Conclusion

The non-adiabatic coupling matrix elements (NACME) for the SF-ORMAS-CI method were derived and implemented in the GAMESS software package. Conventional SF methods have been successfully used in the past to study non-adiabatic processes in quantum chemistry[19–21,23,56,57]; however the large spin contamination inherent in such methods has often proved to be a significant source of error. SF-ORMAS is free of spin contamination, and the availability of NACME greatly expands the applicability of the method, allowing for investigations beyond the adiabatic approximation.

The analytic NACME implementation is tested against two model systems and compared with results from state-averaged CASSCF calculations. The goal of these calculations is not to present any new information on the above systems, but rather to demonstrate the possible suitability of SF-ORMAS in the study of non-adiabatic processes. In all cases, the SF-ORMAS method demonstrates good qualitative agreement with results obtained from CASSCF. While the precise magnitude of the NACME is not expected to be the same among different levels of theory, the NACME computed by SF-ORMAS displays the same general trends as CASSCF along various points on the PES. The data presented here, in conjunction with previously reported results[32,33], strongly suggest that SF-ORMAS is a suitable candidate for the study of non-adiabatic phenomena.

Of course, a more valid test for the current implementation of NACME would be to conduct full non-adiabatic dynamics simulations, either using a surface hopping[8] or an ab-initio multiple spawning[7] approach. This will be the subject of a future study with the SF-ORMAS method. Also of interest is the implementation of the SF-ORMAS gradients and NACME with the effective fragment potential (EFP) solvation method[58]. A previous

implementation of EFP with SF-TDDFT[22] showed promise for the optimization of stationary

geometries and conical intersections of solvated molecules. It will be interesting to examine

the quality of the SF-ORMAS method for the characterization of solvated molecules, and the

effect that spin-contamination may have on such systems. This will also be the subject of a

future study.

Conflict of interest. The authors have no conflict of interest to declare.

7. References

1   M. Born and R. Oppenheimer, Zur Quantentheorie der Molekeln, *Ann. Phys.*, 1927, **389**,

        457–484.

2   W. Domcke, D. R. Yarkony and H. Köppel, *Conical Intersections*, World Scientific, 2004,

        vol. 15.

3   B. H. Lengsfield, P. Saxe and D. R. Yarkony, On the evaluation of nonadiabatic coupling

        matrix elements using SA-MCSCF/CI wave functions and analytic gradient methods. I, *J.

        Chem. Phys.*, 1984, **81**, 4549.

4   N. Matsunaga and D. R. Yarkony, Energies and derivative couplings in the vicinity of a

        conical intersection. II. CH2(2 3A″,3 3A″) and H2S(1 1A″,2 1A″), unexpected results in

        an ostensibly standard case, *J. Chem. Phys.*, 1997, **107**, 7825–7838.

5   S. Matsika, *Conical Intersections*, 2012.

6   D. R. Yarkony, Diabolical conical intersections, *Rev. Mod. Phys.*, 1996, **68**, 985–1013.

7   S. Yang and T. J. Martínez, in *Conical Intersections: Theory, Computation and Experiment*,

        World Scientific, 2011, pp. 347–374.

8   J. C. Tully, Molecular dynamics with electronic transitions, *J. Chem. Phys.*, 1990, **93**,

1061–1071.

9   M. W. Schmidt and M. S. Gordon, The Construction and Interpretation of MCSCF
     Wavefunctions, *Annu. Rev. Phys. Chem.*, 1998, **49**, 233–266.

10   P. G. Szalay, T. Müller, G. Gidofalvi, H. Lischka and R. Shepard, Multiconfiguration Self-
     Consistent Field and Multireference Configuration Interaction Methods and
     Applications, *Chem. Rev.*, 2012, **112**, 108–181.

11   P. Saxe, B. H. Lengsfield and D. R. Yarkony, On the evaluation of non-adiabatic coupling
     matrix elements for large scale CI wavefunctions, *Chem. Phys. Lett.*, 1985, **113**, 159–
     164.

12   B. H. Lengsfield and D. R. Yarkony, On the evaluation of nonadiabatic coupling matrix
     elements for MCSCF/CI wave functions using analytic derivative methods. III. Second
     derivative terms, *J. Chem. Phys.*, 1986, **84**, 348–353.

13   Y. K. Choe, Y. Nakao and K. Hirao, Multireference Møller-Plesset method with a
     complete active space configuration interaction reference function, *J. Chem. Phys.*, 2001,
     115, 621–629.

14   A. I. Krylov, Size-consistent wave functions for bond-breaking: the equation-of-motion
     spin-flip model, *Chem. Phys. Lett.*, 2001, **338**, 375–384.

15   A. I. Krylov, Spin-flip configuration interaction: an electronic structure model that is
     both variational and size-consistent, *Chem. Phys. Lett.*, 2001, **350**, 522–530.

16   A. I. Krylov, Spin-Flip Equation-of-Motion Coupled-Cluster Electronic Structure Method
     for a Description of Excited States, Bond Breaking, Diradicals, and Triradicals, *Acc.
     Chem. Res.*, 2006, **39**, 83–91.

17   D. Casanova and M. Head-Gordon, The spin-flip extended single excitation
     configuration interaction method, *J. Chem. Phys.*, 2008, **129**, 064104.

18   Y. Shao, M. Head-Gordon and A. I. Krylov, The spin-flip approach within time-
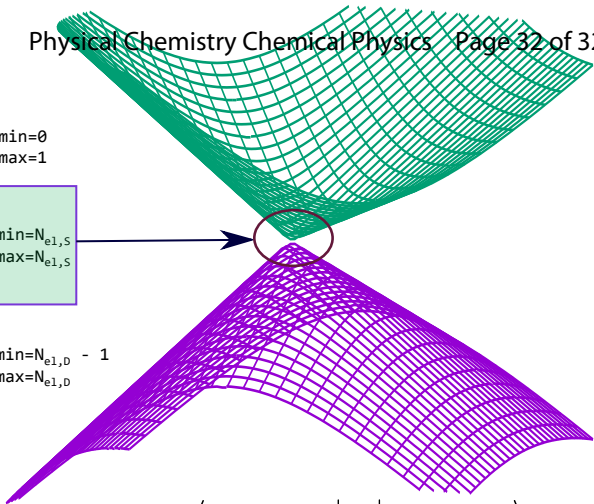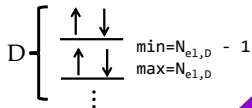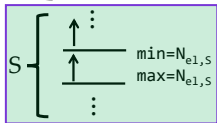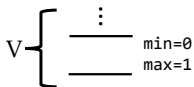
dependent density functional theory: Theory and applications to diradicals, *J. Chem. Phys.*, 2003, **118**, 4807–4818.

19   Y. Harabuchi, K. Keipert, F. Zahariev, T. Taketsugu and M. S. Gordon, Dynamics Simulations with Spin-Flip Time-Dependent Density Functional Theory: Photoisomerization and Photocyclization Mechanisms of cis- Stilbene in ππ* States, *J. Phys. Chem. A*, 2014, **118**, 11987–11998.

20   N. Minezawa and M. S. Gordon, Photoisomerization of Stilbene: A Spin-Flip Density Functional Theory Approach, *J. Phys. Chem. A*, 2011, **115**, 7901–7911.

21   N. Minezawa and M. S. Gordon, Optimizing Conical Intersections by Spin–Flip Density Functional Theory: Application to Ethylene, *J. Phys. Chem. A*, 2009, **113**, 12749–12753.

22   N. Minezawa and M. S. Gordon, Optimizing conical intersections of solvated molecules: The combined spin-flip density functional theory/effective fragment potential method, *J. Chem. Phys.*, 2012, **137**, 034116.

23   X. Zhang and J. M. Herbert, Analytic derivative couplings for spin-flip configuration interaction singles and spin-flip time-dependent density functional theory, *J. Chem. Phys.*, 2014, **141**, 064104.

24   J. S. Sears, C. D. Sherrill and A. I. Krylov, A spin-complete version of the spin-flip approach to bond breaking: What is the impact of obtaining spin eigenfunctions?, *J. Chem. Phys.*, 2003, **118**, 9084–9094.

25   D. Casanova and M. Head-Gordon, Restricted active space spin-flip configuration interaction approach: theory, implementation and examples, *Phys. Chem. Chem. Phys.*, 2009, **11**, 9779.

26   F. Bell, P. M. Zimmerman, D. Casanova, M. Goldey and M. Head-Gordon, Restricted active space spin-flip (RAS-SF) with arbitrary number of spin-flips, *Phys. Chem. Chem. Phys.*, 2013, **15**, 358–366.

27   D. Casanova, Avoided crossings, conical intersections, and low-lying excited states with a single reference method: The restricted active space spin-flip configuration interaction approach, *J. Chem. Phys.*, 2012, **137**, 084105.

28   Z. Li, W. Liu, Y. Zhang and B. Suo, Spin-adapted open-shell time-dependent density functional theory. II. Theory and pilot application, *J. Chem. Phys.*, 2011, **134**, 134101.

29   X. Zhang and J. M. Herbert, Spin-flip, tensor equation-of-motion configuration interaction with a density-functional correction: A spin-complete method for exploring excited-state potential energy surfaces, *J. Chem. Phys.*, 2015, **143**, 234107.

30   Z. Li and W. Liu, Spin-adapted open-shell random phase approximation and time-dependent density functional theory. I. Theory, *J. Chem. Phys.*, , DOI:10.1063/1.3463799.

31   Z. Li and W. Liu, Spin-adapted open-shell time-dependent density functional theory. III. An even better and simpler formulation, *J. Chem. Phys.*, , DOI:10.1063/1.3660688.

32   J. Mato and M. S. Gordon, A general spin-complete spin-flip configuration interaction method, *Phys. Chem. Chem. Phys.*, 2018, **20**, 2615–2626.

33   J. Mato and M. S. Gordon, Analytic Gradients for the Spin-Flip ORMAS-CI Method: Optimizing Minima, Saddle Points, and Conical Intersections, *J. Phys. Chem. A*, 2019, **123**, 1260–1272.

34   M. W. Schmidt, K. K. Baldridge, J. A. Boatz, S. T. Elbert, M. S. Gordon, J. H. Jensen, S. Koseki, N. Matsunaga, K. A. Nguyen, S. Su, T. L. Windus, M. Dupuis and J. A. Montgomery, General atomic and molecular electronic structure system, *J. Comput. Chem.*, 1993, **14**, 1347–1363.

35   M. S. Gordon and M. W. Schmidt, in *Theory and Applications of Computational Chemistry*, eds. Clifford E. Dykstra, K. S. Kim, G. Frenking and G. E. Scuseria, Elsevier, 2005, pp. 1167–1189.

36   J. Ivanic, Direct configuration interaction and multiconfigurational self-consistent-field method for multiple active spaces with variable occupations. I. Method, *J. Chem. Phys.*, 2003, **119**, 9364–9376.

37   B. H. Lengsfield and D. R. Yarkony, in *Advances in Chemical Physics: State-Selected and State-To-State Ion-Molecule Reaction Dynamics, Part 2*, eds. M. Baer and C. Ng, Wiley, 1992, pp. 1–71.

38   Y. Yamaguchi, J. D. Goddard, Y. Osamura and H. F. Schaefer, *A New Dimension to Quantum Chemistry: Analytic Derivative Methods in Ab Initio Molecular Electronic Structure Theory*, Oxford University Press, Oxford, 1994.

39   J. E. Rice, R. D. Amos, N. C. Handy, T. J. Lee and H. F. Schaefer, The analytic configuration interaction gradient method: Application to the cyclic and open isomers of the S3 molecule, *J. Chem. Phys.*, 1986, **85**, 963–968.

40   Y. Yamaguchi, M. Frisch, J. Gaw, H. F. Schaefer and J. S. Binkley, Analytic evaluation and basis set dependence of intensities of infrared spectra, *J. Chem. Phys.*, 1986, **84**, 2262–2278.

41   Y. Osamura, Y. Yamaguchi, P. Saxe, D. J. Fox, M. A. Vincent and H. F. Schaefer, Analytic second derivative techniques for self-consistent-field wave functions. A new approach to the solution of the coupled perturbed hartree-fock equations, *J. Mol. Struct. THEOCHEM*, 1983, **103**, 183–196.

42   P. Saxe, Y. Yamaguchi and H. F. Schaefer, Analytic second derivatives in restricted Hartree–Fock theory. A method for high-spin open-shell molecular wave functions, *J. Chem. Phys.*, 1982, **77**, 5647–5654.

43   N. C. Handy and H. F. Schaefer, On the evaluation of analytic energy derivatives for correlated wave functions, *J. Chem. Phys.*, 1984, **81**, 5031.

44   J. C. Slater, The Theory of Complex Spectra, *Phys. Rev.*, 1929, **34**, 1293–1322.

45   J. C. Slater, Molecular Energy Levels and Valence Bonds, *Phys. Rev.*, 1931, **38**, 1109–
        1144.

46   E. U. Condon, The Theory of Complex Spectra, *Phys. Rev.*, 1930, **36**, 1121–1133.

47   A. C. West and T. L. Windus, Can ORMAS be used for nonadiabatic coupling
        calculations? SiCH 4 and butadiene contours, *Theor. Chem. Acc.*, 2012, **131**, 1–11.

48   C. Galloy and J. C. Lorquet, Nonadiabatic interaction in unimolecular decay. III.
        Selection and propensity rules for polyatomic molecules, *J. Chem. Phys.*, 1977, **67**,
        4672–4680.

49   P. J. Knowles, G. J. Sexton and N. C. Handy, Studies using the CASSCF wavefunction,
        Chem. Phys., 1982, **72**, 337–347.

50   B. O. Roos, P. R. Taylor and P. E. M. Siegbahn, A complete active space SCF method
        (CASSCF) using a density matrix formulated super-CI approach, *Chem. Phys.*, 1980, **48**,
        157–173.

51   B. O. Roos, in *Advances in Chemical Physics*, Wiley, 2007, vol. 69, pp. 399–445.

52   G. Hirsch, P. J. Bruna, R. J. Buenker and S. D. Peyerimhoff, Non-adiabatic coupling matrix
        elements $\langle \Psi z | \partial / \partial Q | \Psi \beta \rangle$ for large CI wavefunctions, *Chem. Phys.*, 1980, **45**, 335–347.

53   M. Barbatti, J. Paier and H. Lischka, Photochemistry of ethylene: a multireference
        configuration interaction investigation of the excited-state energy surfaces., *J. Chem.
        Phys.*, 2004, **121**, 11614–24.

54   N. Minezawa and M. S. Gordon, Optimizing Conical Intersections by Spin - Flip Density
        Functional Theory : Application to Ethylene, *J. Phys. Chem. A*, 2009, **113**, 12749–12753.

55   I. Loaiza and A. F. Izmaylov, On the breakdown of the Ehrenfest method for molecular
        dynamics on surfaces, *J. Chem. Phys.*, 2018, **149**, 214101.

56   S. Gozem, A. I. Krylov and M. Olivucci, Conical intersection and potential energy surface
        features of a model retinal chromophore: Comparison of EOM-CC and multireference

methods, *J. Chem. Theory Comput.*, 2013, **9**, 284–292.

57   X. Zhang and J. M. Herbert, Excited-State Deactivation Pathways in Uracil versus

Hydrated Uracil: Solvatochromatic Shift in the 1 n π* State is the Key, *J. Phys. Chem. B*,

2014, **118**, 7806–7817.

58   P. N. Day, J. H. Jensen, M. S. Gordon, S. P. Webb, W. J. Stevens, M. Krauss, D. Garmer, H.

Basch and D. Cohen, An effective fragment method for modeling solvent effects in

quantum mechanical calculations, *J. Chem. Phys.*, 1996, **105**, 1968–1986.

$$D_{IJ} = \left\langle \Psi_I(r;X) \left| \widehat{\nabla} \right| \Psi_J(r;X) \right\rangle$$